AIChE WILEY InterScience DISCOVER SOMETHING GREAT

BIOENGINEERING, FOOD, AND NATURAL PRODUCTS

Modeling of Freezing Step during Freeze-Drying of Drugs in Vials

Kyuya Nakagawa
Dept. of Mechanical and System Engineering, University of Hyogo, 2167 Shosha, Himeji city, Hyogo 671-2201, Japan

Aurélie Hottot, Séverine Vessot, and Julien Andrieu
Laboratoire d'Automatique et de Génie des Procédés—LAGEP–UMR Q 5007 CNRS UCB Lyon1–CPE, Bât. 308G, 43 Bd du 11 Novembre 1918, 69622 Villeurbanne Cedex, France

DOI 10.1002/aic.11147
Published online March 15, 2007 in Wiley InterScience (www.interscience.wiley.com).

A mathematical model that simulates temperature profiles during freezing process of standard pharmaceutical formulations (mannitol and BSA based) was set up in two-dimensional axsymmetric space, and the ice crystal mean sizes were semi empirically estimated from the resulting temperature profiles. Water vapor mass transfer permeability values during sublimation step were also estimated from ice phase morphological parameters. All these numerical data were compared with experimental data, and a quite good agreement was observed that confirmed the adequacy of the present model calculations. It was confirmed that, for a given formulation, the mass transfer parameters during freeze-drying were strongly dependent on morphological textural parameters, and consequently, on the nucleation temperatures that fix the ice phase morphology. The influence of freezing rate was also predicted from the simulations, proving that an increase of cooling rates led to slower primary drying rates. © 2007 American Institute of Chemical Engineers *AIChE J,* 53: 1362–1372, 2007
Keywords: nucleation temperature, freeze-drying, ice crystal morphology, freezing modeling

Introduction

To optimize freeze-drying processes, the freezing step has a critical importance because subsequent ice sublimation rates are strongly related with ice crystal morphology and corresponding textural and structural parameters are mostly fixed during freezing step. Thus, as it concerns optimization of the freezing step, the control of ice crystal morphology (i.e. ice crystal mean sizes, ice crystal shapes, ice crystal size distribution, etc.) is a major challenge for freeze-drying process optimization.

It is known as a general trend that cooling rates are the key factors of freezing processes because large ice crystals results from slow cooling rates, while faster cooling rates lead to smaller and more numerous ice crystals. Moreover, the ice crystal sizes are strongly related to the rates of crystal growth, which are governed either by the mass transfer of water or by the heat transfer throughout the system. The influence of freezing step parameters on the subsequent sublimation characteristics was precisely investigated by Kochs et al.[1] As main result, these authors concluded that a decrease of cooling rates led to a significant increase of water vapor mass transfer rates during sublimation, which finally reduced the freeze-drying times. Furthermore, these authors succeeded in directly correlating the freezing conditions to the mass transfer phenomena taking place during freeze-drying.[2] Nevertheless, these authors mentioned that nucleation temperature could not have great impact on a macroscopic sample freezing, which was controlled mainly by cooling conditions and not so much influenced by initial temperature distributions. In case of small scale frozen systems like standard pharmaceutical freeze-drying in vials, the

Correspondence concerning this article should be addressed to J. Andrieu at andrieu@lagep.cpe.fr.

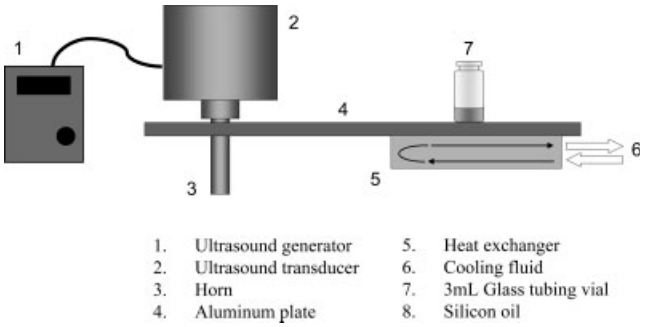

Figure 1. The cooling device coupled with ultrasound system.

influences of latent heat generated by nucleation and ice crystal growth, the heat transfer between sample and ambient air, as well as the sample geometry have to be taken in account. Thus, for small scale frozen system, many authors consider the nucleation temperature as a key factor for the optimization of principal quality factors. As a matter of fact, the undercooling degree of the solution determines the number of nuclei and, consequently, greatly influences the ice crystals morphology in the frozen sample.[3] Searles et al. in the study of freeze-drying of aqueous standard diluted formulations used as model systems for pharmaceuticals proteins freeze-drying in vials experimentally observed that some ice morphology characteristic parameters and, by the way, primary drying rates were quite correlated with nucleation temperatures, i.e., to undercooling degrees and to thermal gradients in the system.[4] However, ice nucleation is well known to be a spontaneous and stochastic phenomenon more or less related to material and process parameters that are generally difficult to control like impurities, asperities, surface roughness. Consequently, it appears important to investigate relationships among morphological parameters of the ice phase, primary drying times, and freezing conditions.

In this article, a mathematical model of freezing process was proposed, and the temperature profiles of standard pharmaceutical formulation (mannitol and BSA based) were simulated by using the commercial finite element code FEMLAB in two-dimensional axsymmetric space taking account of actual vial geometry and freeze-drying operating conditions. From calculated experimental temperatures profiles, a semi-empirical model was set up to estimate the mean ice crystal size and, consequently, the water vapor dried layer permeability. Finally, these numerical results were compared to experimental data.

Experiment

Materials

Two types of standard simplified formulations generally selected for heat sensitive pharmaceutical proteins freeze-drying were successively investigated, namely:

- 10% mannitol solution prepared from distilled water and mannitol powder (Fluka Chemie AG), which corresponded to a crystalline system.
- 5% BSA (Bovin Serum Albumin) type formulation (Sigma Aldrich), which corresponded to an amorphous system.

Freezing procedure

Tubing glass vials (Verretubex, France) of 3 mL (vial diameter $D = 12$ mm) were used in this work. Sample solution (0.75 mL) was filled in each vial (height $h = 7$ mm in solution; $h = 8$ mm in frozen state) and the sample temperatures were monitored by type K thermocouples. Sensitive extremities of these thermocouples were attached by pads (COMARK) on the exterior surface of each vial wall, at mid-

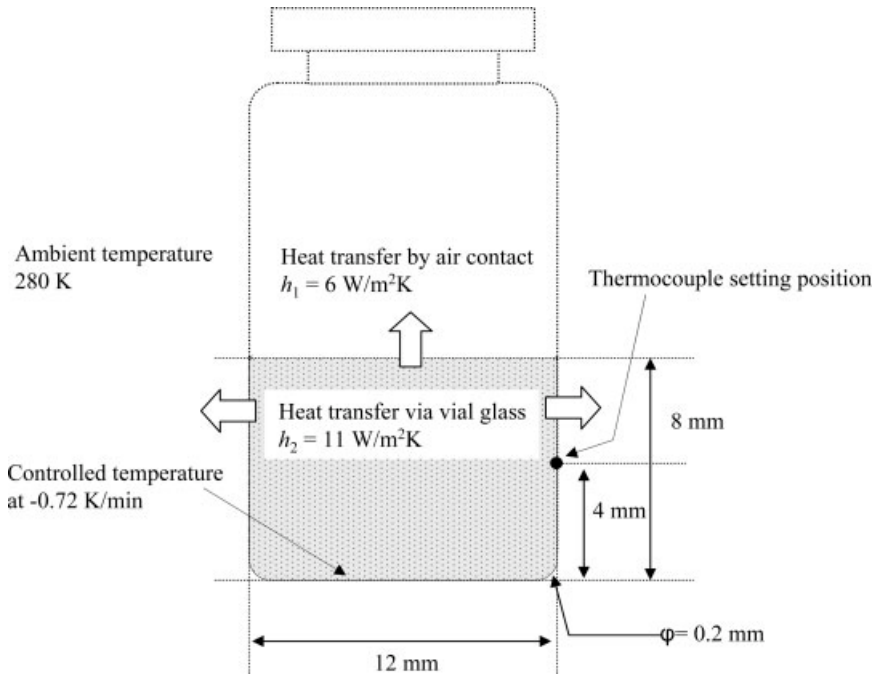

Figure 2. Scheme of the sample geometry.

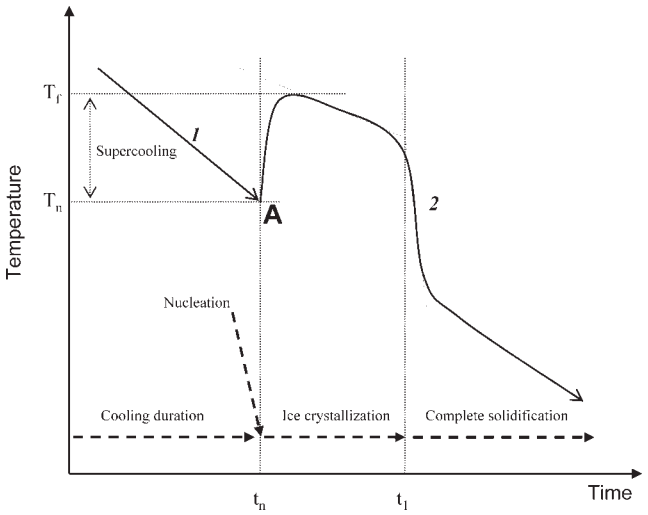

Figure 3. Scheme of temperature profile during cooling and freezing steps.

dle height position between liquid meniscus and vial bottom, i.e. at about 4 mm from the vial bottom. By this external noninvasive fixing, the nucleation phenomena were not submitted to any artifact that usually results from the introduction of thermocouples inside the vial. Besides, an adequate thermal paste (TECHSPRAY) was used for improving thermal contact between thermocouple sensitive part and external surface of the vial glass wall. Then, sample temperatures were stored and recorded with a data acquisition system (4100G Eurotherm Recorders) every 2 s.

To trigger and to control the nucleation processes, the cooling device was combined with the ultrasound transducer (SODEVA, France) as illustrated in Figure 1.[5] An ultrasound transducer was tightly attached to an aluminum plate (200 $\times$ 200 mm^2, 5 mm thickness) by clamping the aluminum plate itself to a horn of the transducer. Furthermore, the same transducer was coupled with an ultrasound generator (MW400GSIP, SODEVA, France) and the frequency of the vibration was tuned up around 35.89 kHz in order to obtain an adequate frequency resonance on the aluminum plate. The aluminum plate was placed in thermal contact as close as possible with the aluminum heat exchanger (width 300 mm, length 100 mm, height 10 mm) by clamper fixing. A cooling fluid (Therminol D12, Solutia) was circulated through the heat exchanger at precisely controlled temperatures with a thermo regulated cryofluid bath (CC180, Huber, Germany). Then, the liquid solution samples were introduced inside the vials and the vials were placed on the aluminum plate. Because of ultrasound vibrations on the plate and to resonance phenomena, nodal points existed all through the plate surface. The places of these nodal points should be avoided for the vial setting because, at these points, the ultrasound vibrations could not propagate at all inside the vial solution volume. Moreover, to enhance this propagation, a thin layer of silicon oil was inserted between the curved vial bottom and the aluminum plate, because without this contact fluid, the ultrasound waves could not efficiently propagate all through the whole vial solution and, furthermore, in absence of silicon oil, vibration causes the vials to slip and eventually be overturned; the presence of silicon oil hinders such undesired effects.

Sample vials were put on the precooled cold stage (at 7°C), and then, after 5 min, the cooling rate of the cryofluid circulating through the heat exchanger was adjusted at −1°C/min up to −45°C. The corresponding actual cooling rate of the sample solution was equal to the −0.72°C/min at the vial bottom. This value was used for the model calculation presented hereafter.

Direct observation of ice crystals morphology

The ice crystal morphology was analyzed by photonic microscopy method by reflexion with episcopic coaxial lighting. This method is essentially based on the light flux reflected by the surface of the sample and has the main advantage to preserve at best the original structure of the frozen sample as proposed by Faydi et al.[6,7] in the case of frozen foods (ice creams) structure analysis. The direct observation was realized in cold chamber maintained at −25°C where the microtome (LEICA 2000R), the microscope (LEICA MZ12), the digital camera (Hitachi CCD), and an optical fiber providing the episcopic coaxial lighting were placed. The frozen sample prepared as described earlier was taken out by breaking off the glass vial; then it was carefully fixed on a metal support by tissue freezing medium (LEICA Instruments GmbH) and finally stored in liquid nitrogen. Before the observation, the sample was cut with a microtome and carefully smoothed down to obtain a surface roughness lower than 1 μm. The obtained images were numerically stored in the computer and then were analyzed by Image J 1.34 software that allowed the estimation of equivalent and mean particle sizes.

Freeze-drying procedure

Frozen samples were freeze-dried (sublimation period) with a laboratory pilot freeze-dryer (USIFROID SMH45, France) with the following protocol.[8,9]:

- Vials with frozen samples placed on the precooled shelf at −40°C inside the freeze-dryer chamber;

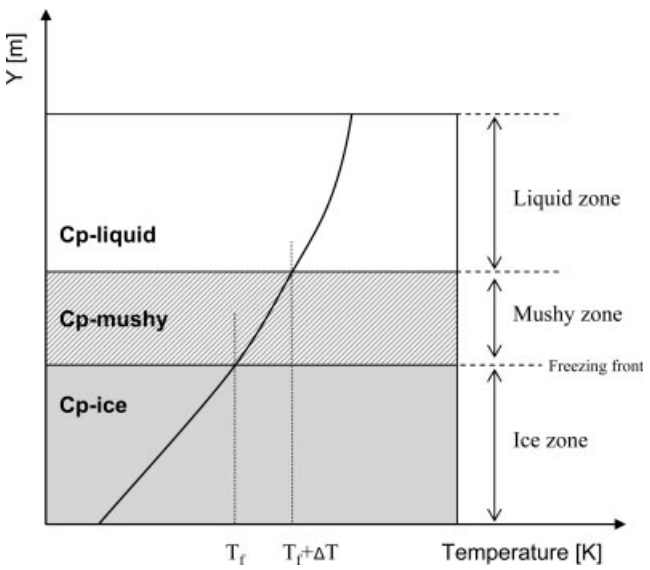

Figure 4. Model of the physical formulation states through the sample.

Table 1. Numerical Values Used in the Calculation

		10% Mannitol	5% BSA
Model calculation	k_{liquid} (W/m K)	0.6	0.6
	k_{ice} (W/m K)	2.5	2.5
	$C_{p\text{-liquid}}$ (J/kg K)	3852	4020
	$C_{p\text{-ice}}$ (J/kg K)	1967	2030
	T_f (K)	270.3	271.4
	ΔH_f (J/kg)	333500	333500
	ΔX_{ice}	0.9	0.9
	ΔT (K)	0.98	0.98
Ice crystal size estimation	a	12	22
Permeability estimation	ε/τ	0.225	0.112

• Vacuum setting inside the freeze-dryer sublimation chamber at $P_c = 10$ Pa;

• Increase the shelf temperature from -40 to -20°C at 1°C/min;

• Maintain steady freeze-drying conditions all along during the primary drying period.

A set of 30 vials was placed on the shelves in the same locations in a cubic arrangement for all runs, and two or three runs were repeated for each set of freeze-drying conditions. To determine the primary drying rates, the freeze-drying run was stopped after 3–4 h of sublimation that corresponded to 30–40 wt % of ice sublimated and the weight loss was measured.

Model calculation

The 2D axisymmetric model taking into account the real geometry of the vial was written under FEMLAB 3.0 (COMSOL), which is a software dedicated to simulate complex heat and mass transfer phenomena. An interesting advantage of this software is the possibility of taking account of the actual sample geometry on the CAD interface, and of the corresponding boundary conditions expressed by heat flux continuities, heat losses, etc.[10] With this approach, the integration domains are divided as triangles and the side of the meshes can be more or less curved dependent on the geometry. The grid mesh size and the number of elements can be selected in each simulation model calculation.

Model geometry was created on FEMLAB 3.0 as illustrated in Figure 2 in order to simulate freezing phenomena in a vial submitted to our selected experimental conditions. For our calculations, we chose refined mesh with 3784 elements.

Modeling the freezing step

Temperature profile during freezing process is schematized in Figure 3. First, the sample was cooled down at constant cooling rate until some supercooled level at which nucleation started, and then, the temperature increased rapidly due to latent heat generated by nucleation up to the equilibrium freezing temperature; next the temperature decreased moderately due to the latent heat generated by the ice crystal growth up to the end of ice crystal growth period corresponding to total ice freezing, and then continued to decrease until complete solidification of cryoconcentrated phase. We have to point out that the ice crystals morphology generally depends on the place where nucleation starts, so that we adopted the hypothesis that nucleation always started at the bottom of the vial. This hypothesis seems realistic because we could experimentally observe this phenomenon on our freezing system where ultrasound device was used for nucleation control. It should also be observed that there were always temperature gradients in the present system throughout the liquid (especially, perpendicular to the cooling plate), thus, this undercooling and temperature gradients determine the nucleation processes and crystal growth rate, and then, the ice crystal growth progressed moderately.

To simulate these freezing temperature profiles, our modeling was divided into two periods, namely the cooling step (1) and then the freezing step (2) as explained later.

Cooling step

It was necessary to simulate the cooling step in order to obtain the initial condition for the temperature profile throughout the vial bulk for the subsequent freezing step. Thus, the cooling step from $t = 0$ to the nucleation time noted, t_n, was simulated with the following conditions:

• $t = 0$: the temperature throughout the vial was uniform and equal to 15°C.

• $t = 0$–300s : the vial bottom was in contact with the plate maintained at the constant temperature equal to 7°C.

• $t = 300$ to t_n: the vial bottom was cooled down at the cooling rate at -0.72 K/min.

The basic equation of cooling step modeling was the conductive heat equation (second Fourier's law) applied all through the formulation volume, namely:

$$\rho C_{p-\text{liquid}} \frac{\partial T}{\partial t} = \nabla(k \nabla T) \tag{1}$$

Because of quite small temperature ranges involved during this period (ΔT range between 25 and 50 K), we assumed that the solution density and specific heat capacity values were constant all along the solution cooling. These assumptions were also adopted in the freezing step modeling.

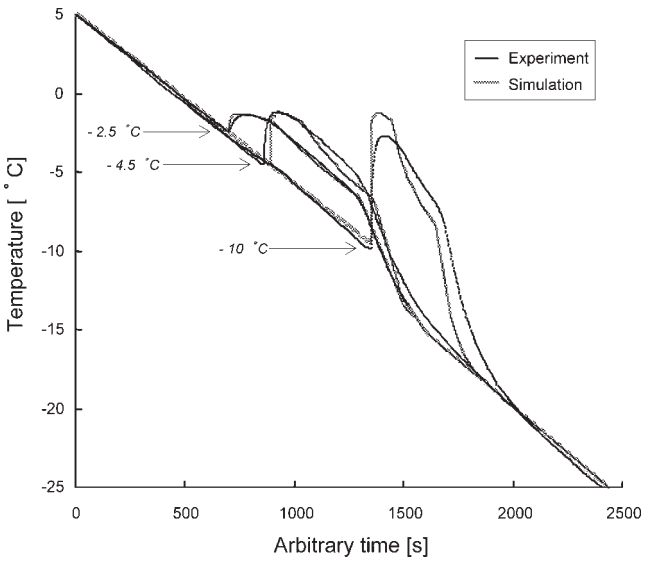

Figure 5. Experimental and simulated temperature profiles during cooling and freezing.

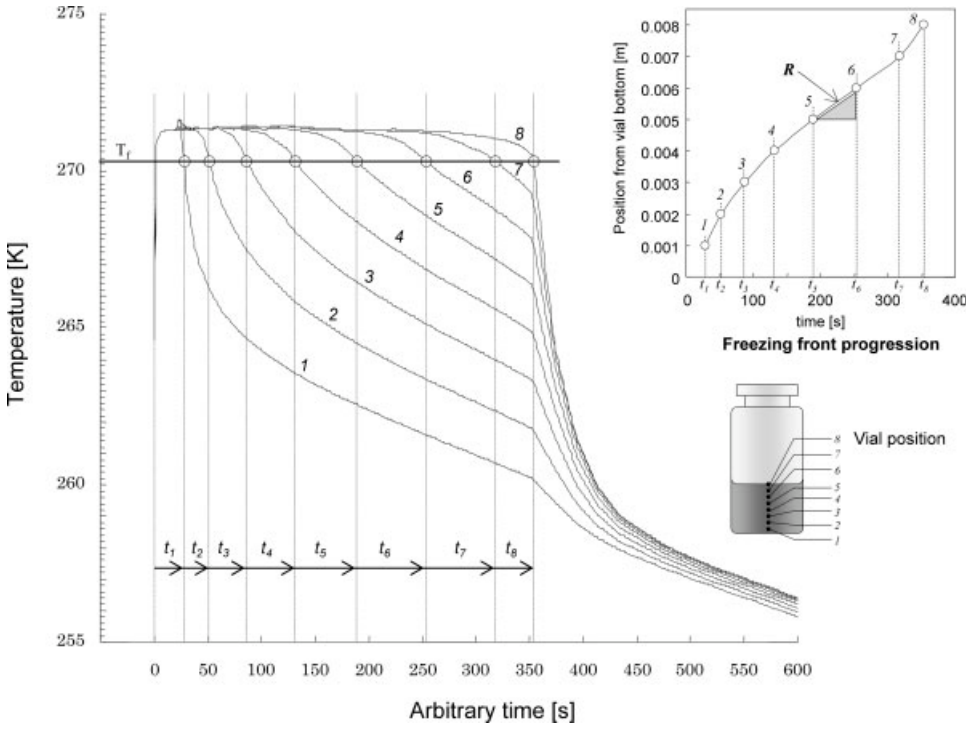

Figure 6. Estimation of freezing front rate, *R* (T_n = −7°C; mannitol).

Freezing step

During the freezing step, first nucleation started at the fixed time t_n corresponding to nucleation temperature, T_n, and subsequently, ice crystal growth progressed moderately. Generally speaking, it is not possible to predict nucleation temperature (as mentioned in present paper), and so a nucleation temperature has not been regarded as a fixed parameter in the model. However, in our paper, an ultrasound device was set up to fix the ice crystal nucleation temperature, thus, we could put it in a model as the most critical parameter. Our model is a combination of two main works: a model on ice crystal growth in homogeneously undercooled liquid by Qin et al.[11]; and a model of uniformed ice crystal growth regardless of supercooling by Lunardini.[12] We combined these two main ice crystal growth models, and introduced a nucleation temperature as a key parameter that fixes the corresponding temperature gradients and ice crystal growth rates. The freezing modeling was based on the heat conduction equation recalled below with two source terms, namely the heat generation due to the ice nucleation latent heat, $\dot{Q}_n$, and the heat generation due to the ice crystallization latent heat, $\dot{Q}_c$.

$$\rho C_{p-\text{apparent}} \frac{\partial T}{\partial t} = \nabla(k\nabla T) + \dot{Q}_n + \dot{Q}_c \tag{2}$$

It was assumed that the rate of ice nucleation was proportional to the supercooling degree $T_f - T^*$, so that the positive source term $\dot{Q}_n$ was expressed as follows[11]:

$$\dot{Q}_n = \Delta H_f k_i (T_f - T^*) \tag{3}$$

where T^* represents the temperature in the supercooled liquid and T_f, the freezing front temperature. This term became zero as soon as the supercooled water has totally been crystallized. Nucleation rate constant k_i [kg/(m^3 s K)] could be estimated from freezing front velocity v (m/s), namely:

$$k_i = \frac{v\rho}{s(T_f - T^\circ)} \tag{4}$$

Here, T° represents homogeneous undercooled temperature and, s the thickness of the undercooled zone. If we assume

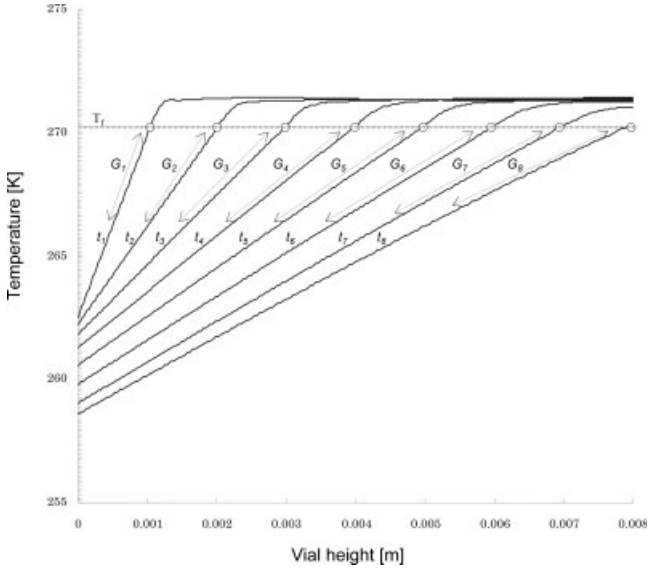

Figure 7. Estimation of temperature gradients in frozen zone, *G* (T_n = −7°C; mannitol).

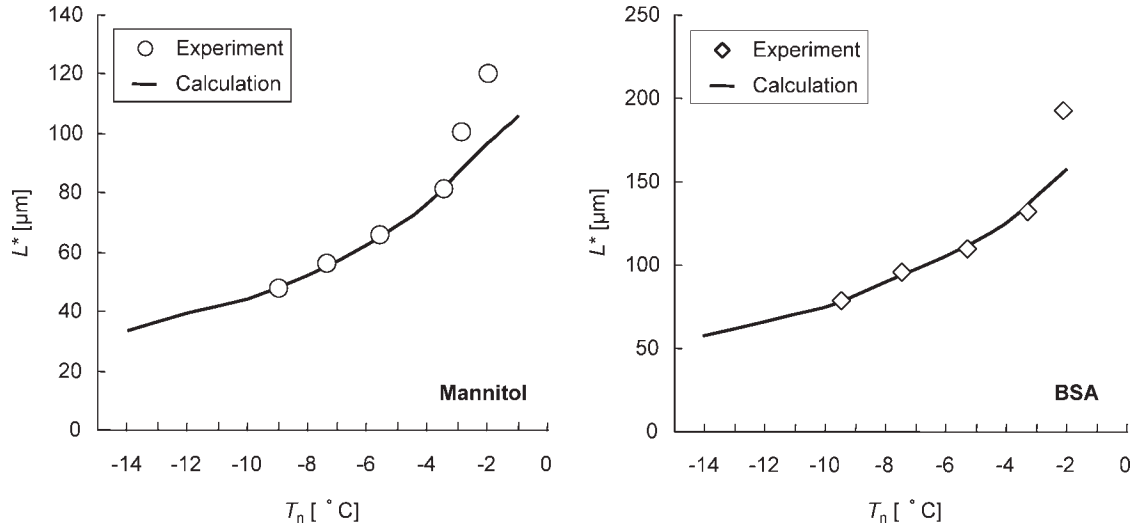

Figure 8. Ice crystal mean sizes as a function of nucleation temperatures.

$v = 0.0085$ m/s,[13] $s = 3$ mm, and $(T_f - T^\circ) = 10$ K as mean standard values, we obtained $k_i = 430$ kg/(m^3 s K); this estimated value of k_i was assumed constant all along the freezing step. The value $(T_f - T^\circ) = 10$ K was a mean value for the supercooling degree of present system, which was obtained from the frequency of spontaneous nucleation temperatures data measured by authors.

Besides, the positive source term, $\dot{Q}_c$ corresponding to the latent heat generated by the ice crystallization was expressed by the classical equation:

$$\dot{Q}_c = \Delta H_f \frac{\partial}{\partial t}(\rho X_{ice}) \tag{5}$$

As illustrated in Figure 4, during the ice crystal growth period, the sample could be divided in three zones corresponding to three different physical states, namely, a solid zone, a mushy zone, and a liquid zone. The mushy zone is a suspension of ice in the undercooled solution (ice fraction, X_{ice}) which was defined by the temperature difference (ΔT) between the freezing front and the liquid zone. This ΔT parameter was a fitting parameter, the value of which was identified from experimental data. Moreover, supposing that the ice crystal growth rate was entirely controlled by the heat transfer and that the ice fraction, X_{ice}, varied linearly with the temperature in the domain of phase change, the expression of this source term could be written as follows[10]:

$$\Delta H_f \frac{\partial}{\partial t}(\rho X_{ice}) = -\Delta H_f \rho \frac{\partial X_{ice}}{\partial T}\frac{\partial T}{\partial t} = -\Delta H_f \rho \frac{\Delta X_{ice}}{\Delta T}\frac{\partial T}{\partial t} \tag{6}$$

Thus, this term could be introduced in the accumulation term by using an apparent heat capacity value, $C_{p\text{-apparent}}$, defined as follows.[12]

$$\rho C_{p-apparent} = \begin{cases} C_{p-liquid} : T > T_f + \Delta T \\ \dfrac{C_{p-liquid} + C_{p-ice}}{2} + \dfrac{\Delta H_f}{\Delta T}\Delta X_{ice} : T_f \le T \le T_f + \Delta T \\ C_{p-ice} : T < T_f \end{cases} \tag{7}$$

The variations of apparent thermal conductivity and of bulk density values as a function of temperature were represented by a linear law all along the domain between the liquid and the solid zone.[13] The parameters used in this simulation are gathered in Table 1 hereafter.

Boundary conditions

As illustrated in Figure 2, at the boundary of the sample, the following conditions were assumed.

- Ambient temperature, $T_{ambient} = 280$ K.
- Convective heat transfer between air and vial glass, $h_1 = 11$ W/(m^2 K).[10,14]
- Convective heat transfer between air and the liquid zone top, $h_2 = 6$ W/(m^2 K).[10,14]

These heat transfer coefficient values were introduced in the following equations, which express the heat flux continuity at the sample wall boundary:

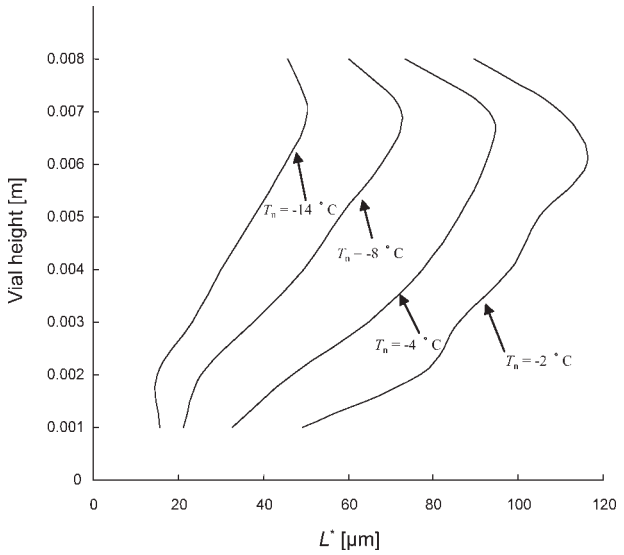

Figure 9. Simulation of ice crystal size distributions in vial vertical direction (mannitol).

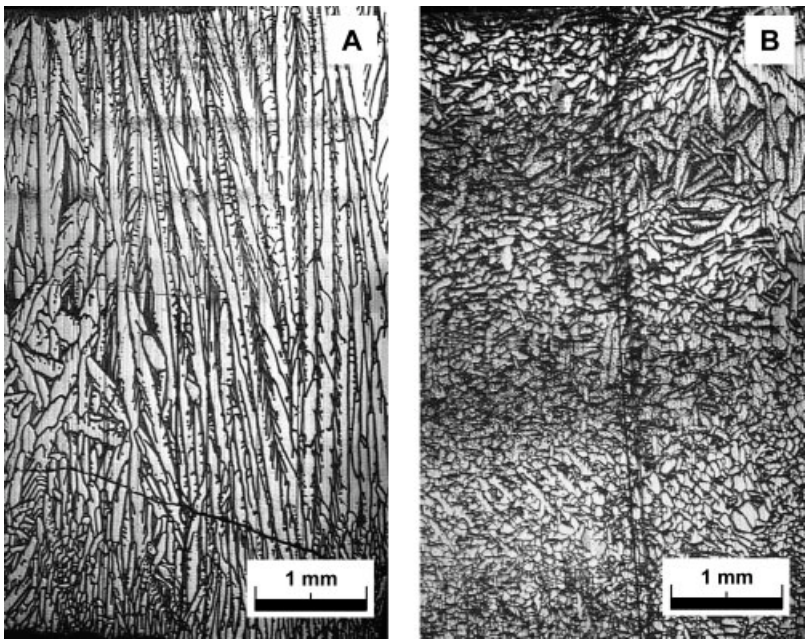

Figure 10. Microscopic images of vertical sample cuts (10% mannitol): (A) nucleated at −2.04°C; (B) nucleated at −7.39°C.

$$-k\frac{\partial T}{\partial t} = h(T - T_{\text{ambient}}) \tag{8}$$

Finally, we assumed that the temperature decreasing rate at the sample bottom was always constant and equal to −0.72 K/min corresponding to the chosen cryofluid cooling rate as mentioned earlier.

Results and Discussions

Freezing curves

Based on the equations presented earlier, cooling and freezing temperature profiles were calculated as a function of selected nucleation temperatures. To unify the experimental temperature profiles measured by a thermocouple set on the vial external surface, the nucleation temperature, T_n, was defined as the minimum undercooled temperature at the point A (*cf.* Figure 3) corresponding to the nucleation time, $t = t_n$.

Comparison of experimental and calculated freezing curves in Figure 5 shows good agreements between both series of temperature profiles. The deviation between the profiles nucleated at about −10°C was larger than that for the other profiles. However, all these data seems enough precise to allow the determination of the ice crystal growth rates and of the temperature gradients in the sample in order to estimate ice crystal mean sizes on this literature reviewed.

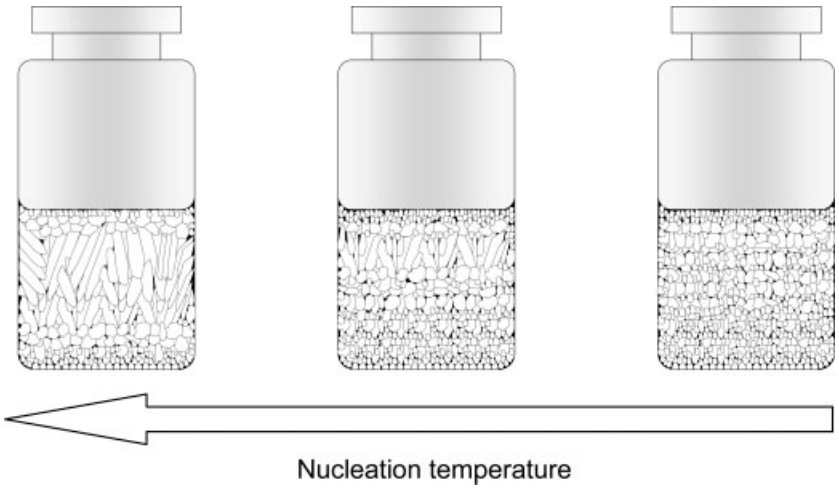

Figure 11. Sketches of ice crystal morphologies.

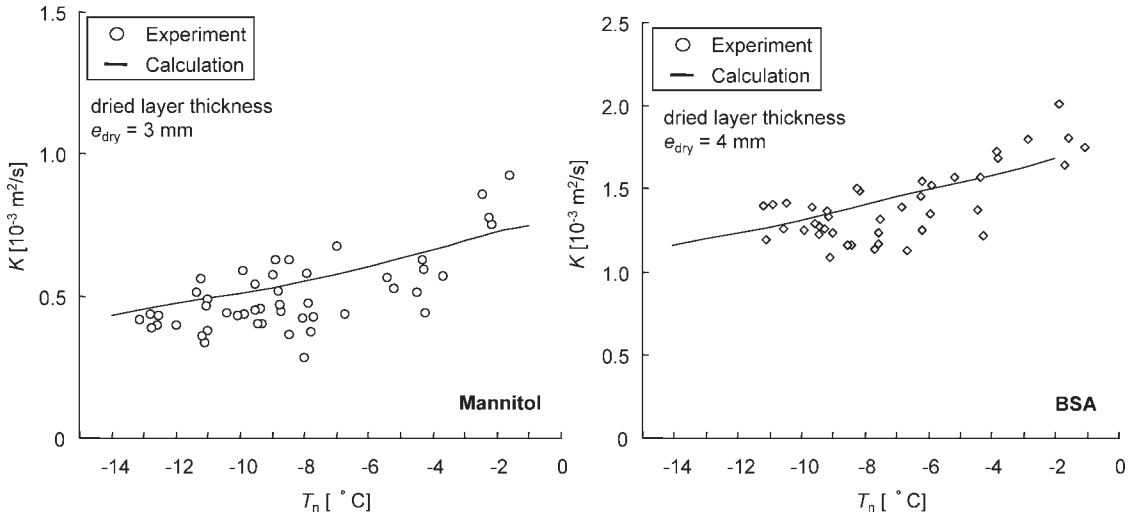

Figure 12. Comparison of experimental and estimated dried layer permeability.

Estimation of mean ice crystal sizes

Several research works have been devoted to establish quantitative relationship between ice crystal mean size, L^*, and overall freezing parameters like the freezing front rate, R, and the temperature gradient in frozen zone, G. For example, Kurz and Fisher[15] proposed the following correlation type $L^* \propto R^{-1}G^{-1}$ or $L^* \propto R^{-0.5}$ for metal solidification system at low rates. In the food domain, Bomben and King[16] proposed the relation $L^* \propto R^{-0.5}G^{-0.5}$ in the case of apples. From the starch gels, Reid[17] proposed the correlation type $L^* \propto R^{-x}$, meanwhile, Kochs et al.[1] confirmed the correlation proposed by Kurz for alloy solidification at high rates, namely $L^* \propto R^{-0.25}G^{-0.50}$. Woinet et al.[18] obtained relation types as $L^* \propto R^{-1}$ or $L^* \propto R^{-0.5}G^{-0.5}$ for unidirectional freezing of gelatin gels.

Based on this literature review and due to our ice phase morphology type, we adopted the following relationship type in order to interpret our ice morphology data:

$$L^* = aR^{-0.5}G^{-0.5} \tag{9}$$

where, a (ms/K) is an empirical constant that was identified by experimental data.

The R values were estimated from temperature profiles at different location (each 1 mm) from the vial bottom as shown in Figure 6. For each position (l_i), the time (t_i) corresponding to the freezing front passing across was determined at the equilibrium freezing temperature (T_f).

The G values were estimated from temperature profiles at each selected time (t_i). As shown in Figure 7, the frozen zone temperature profiles, that corresponds to the region for which temperature values are lower than T_f, gives directly the temperature gradient value, G.

Calculated mean ice crystal sizes values (L^*) of frozen mannitol and BSA formulations are plotted as a function of nucleation temperatures, and compared with the values obtained from image analysis in Figure 8. The identified values of parameter, a, used to obtain the presented plots are gathered in Table 1. Although some deviations were observed around $T_n = -2^\circ$C, most of other data are in quite good agreement. These calculated data are mean values obtained by averaging local ice crystal sizes throughout the whole sample bulk. Moreover, estimated ice crystal size distributions as a function of location are plotted in Figure 9. From this figure we observed that the ice crystal sizes generally increase as a function of vial height, if we except the top layer of the vial where the ice crystal sizes become smaller. This tendency was more pronounced with the sample that nucleated at higher temperatures corresponding to lower supercooling degrees. Moreover, this behavior was qualitatively confirmed by the images of ice crystals morphology shown in Figure 10, and it has also been reported on previous studies on freeze-drying primary drying.[19] It can be concluded that these images support and confirm the modeling data plotted in Figure 9, as summarized in the sketch in Figure 11.

Estimation of freeze-dried layer permeability

As shown in the previous sections, we could estimate the ice crystal mean sizes as a function of nucleation temperatures. To interpret the dependency of the ice crystal morphologies on the sublimation rates, we have estimated the water vapor mass transfer permeability of the dried layer as the last step of our modeling approach. As a matter of fact, the increase of the nucleation temperature was expected to increase the water vapor mass transfer permeability of freeze-dried materials and to contribute to accelerate the primary sublimation rates during freeze-drying.

Water vapor permeability, noted K, was defined by following equation:

$$\overline{m} = \frac{KM_w}{R_g T}\,\mathrm{grad}P \tag{10}$$

Thus, from this relation the experimental K values could be approximately estimated from experimental value of the primary drying rate, $\overline{m}$, over the sublimation period corresponding to the dried layer thickness, e_{dry}, by following relation:

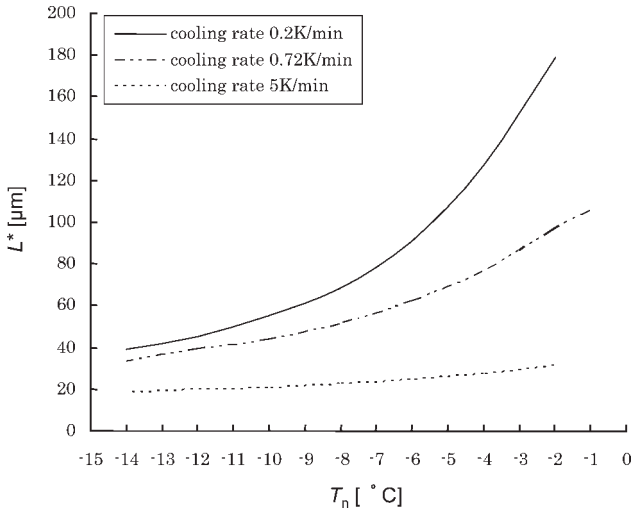

Figure 13. Simulation of influence of cooling rates on ice crystal mean sizes (mannitol).

We can observe a quite good agreement in Figure 12 between K_{exp} and K_{model} values estimated from each data set. These plots show clearly that water vapor mass transfer resistances decrease as the nucleation temperatures increases, so that the drying rates were accelerated by increasing the nucleation temperatures. This tendency is in logical agreement with the ice crystal size estimation obtained both from image analysis and from model calculation presented in the previous paragraph. Consequently, it is confirmed that, for a given system, the mass transfer phenomena during freeze-drying are strongly dependent on frozen formulation morphologies. On the other hand, one can observe from these figures the strong relationships between K values and nucleation temperatures for each data set. Thus, we can conclude that the freezing conditions really fixed the permeability of the dried layer during the sublimation step.

Moreover, these data confirm the adequacy of our model to estimate ice crystal morphological parameters, and consequently, the water vapor permeability of the dried layer during the sublimation step of pharmaceuticals freeze-drying in vials.

$$K_{exp} = \frac{e_{dry}}{P_s - P_c}\frac{R_g T_s}{M_w}\cdot \overline{m} \tag{11}$$

As mentioned previously, we calculated primary dying rates from the weight loss during 3–4 h of sublimations. The K_{exp} values plotted in Figure 12 corresponded to mean values of dried layer thickness, e_{dry}, were about 3 and 4 mm for mannitol and BSA system, respectively.

Besides, dried zone permeability, K, can be also theoretically estimated from mean ice crystal values by assuming that the dried cake texture is represented by a bundle of capillary tubes (diameter $\overline{d}_p$). In our case, we could estimate the value of Knudsen number around $K_n = 4$, consequently, and from the molecular diffusion theory in Knudsen regime, the dried layer permeability, K, by the following equations[20]:

$$K_{model} = \frac{\varepsilon}{\tau} D_k \Omega \tag{12}$$

where the Knudsen diffusivity is expressed by:

$$D_k = \frac{1}{3}\sqrt{\frac{8R_g T_s}{\pi M_w}}\cdot \overline{d}_p \tag{13}$$

and the total flow contribution factor, Ω, is equal to:

$$\Omega = \frac{1}{1 + \overline{d}_p/\lambda} \tag{14}$$

where λ represents the mean free path, given by:

$$\lambda = \frac{k_b T_s}{\sqrt{2}\pi d_m^2 P} \tag{15}$$

For this estimation, we assumed that the mean ice crystal sizes corresponded to the pore diameter ($\overline{d}_p$) in the Eqs. 13 and 14. In Eq. 12 the form factor ε/τ is an empirical constant that was identified from experimental data, and those values are listed in Table 1.

Influence of cooling rates

As discussed previously, it is clear that nucleation temperatures are key parameters that determine the ice morphology and, consequently, the sublimation times during freeze-drying processes. Because of spontaneous and stochastic nature of nucleation phenomenon, it is not easy to practically control this parameter. Nevertheless, an ultrasound system was able to trigger the nucleation process in vial freeze-drying process as previously reported by authors.[5] However, as mentioned earlier, it is the cooling rate that is the easiest freezing operating parameter that influence on the ice crystal morphology. This is why the influence of the cooling rate on ice crystal sizes and dried layer permeability was estimated with our modeling as a function of nucleation temperature. These pre-

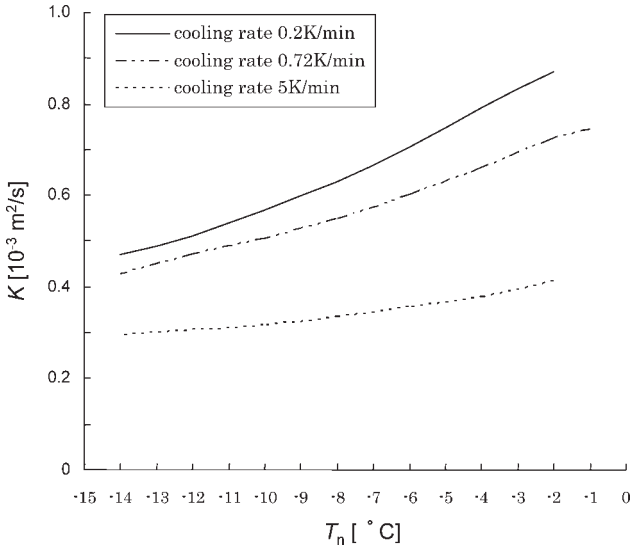

Figure 14. Simulation of influence of cooling rates on dried layer permeability (mannitol).

dictions would be very useful, though the corresponding experimental data were very difficult to obtain.

Figure 13 shows the estimated ice crystal mean sizes simulated for different cooling rates; the estimation was executed with mannitol samples and used the same values for the empirical constant (a and ε/τ) reported in Table 1. These simulation results clearly show that an increase of cooling rate leads to smaller ice crystal sizes. Moreover, it is noteworthy that this tendency becomes much more marked by increasing the nucleation temperature increase, so that the ice crystal size dependency on the nucleation temperatures becomes much higher by decreasing the cooling rate. For example, when samples were prepared at cooling rate equal to -5 K/min (fast cooling), the variation of nucleation temperature does not result in too large distribution of ice crystals. Consequently, it is predicted relatively uniformed sublimation rates though their corresponding sublimation rates would be very slow as shown in Figure 14. Finally freeze-dried layer permeability values calculated from these data (Figure 14) clearly explain the influence of freezing protocol on the sublimation step duration.

Conclusion

A mathematical modeling for a standard pharmaceutical formulation (mannitol and BSA based) freezing process was proposed by using the commercial finite element code FEMLAB in two-dimensional axsymmetric space. Those data were compared to experimental data obtained with the same geometry and the same operating conditions. Calculated freezing curves were found in fine agreement with experimental data, and then, ice crystal mean sizes estimated from the obtained temperature profiles were also confirmed by experimental values. Ice crystal size distributions in vertical direction were quantitatively predicted by the model calculation, and these characteristics were supported by optical microscopy images. It was suggested that the ice crystal sizes increase as a function of cooled bottom distance; however, at the top layer of the vial, ice crystal sizes become smaller. This tendency was much more pronounced with the samples that nucleated at higher temperature. Based on molecular diffusion theory, dried layer permeability was estimated from simulated ice crystal sizes and we observed a satisfactory agreement between experimentally determined values and the values estimated from ice crystal sizes. Consequently, it was confirmed that, for a given system, the mass transfer parameters during freeze-drying were strongly dependent on the textural and morphological parameters of ice phase, and consequently, on the nucleation temperatures. The simulation data for different freezing rates predicted that the increase of cooling rates led smaller ice crystal sizes. Moreover, it is noteworthy that this trend becomes much more marked as the nucleation temperature increase, and that the ice crystal size dependency on the nucleation temperature becomes higher by decreasing the cooling rate. Dried layer permeability calculated from these data also explained the influence of freezing rates on duration of the sublimation step. Thus, by increasing the cooling rates we obtained slower primary drying rates related to lower nucleation temperatures. Finally, it is expected that the present modeling and experimental approach could help the optimization of pharmaceuticals freeze-drying cycles in industrial conditions.

Acknowledgments

This work is supported by a grant from Japan Society for the Promotion of Science.

Notation

a = Empirical parameter in Eq. 9
C_p = Heat capacity (J/(kg K)
D_k = Knudsen molecular diffusion coefficient (m^2/s)
d_m = Diameter of water molecule (m)
d_p = Pore diameter (m)
$\overline{d}_p$ = Ice crystal mean diameter (m)
e_{dry} = Dried layer thickness (m)
G = Temperature gradient in frozen zone (K/m)
ΔH_f = Latent heat of crystallization (J/kg)
h = Convective heat transfer coefficient (W/(m^2 K))
K = Dried layer permeability (m^2/s)
k = Thermal conductivity (W/(m K))
k_B = Boltzmann constant (J/K)
k_i = Nucleation rate constant (kg/(m^3 s K))
K_n = Knudsen number
L^* = Ice crystal mean size (m)
M_w = Molecular weight of water (kg/kmol)
$\overline{m}$ = Water vapor sublimation rate (kg/(m^2 s))
P = Total pressure (Pa)
P_c = Chamber total pressure (Pa)
P_s = Sublimation front total pressure (Pa)
Q_c = Latent heat of crystallization (W)
Q_n = Latent heat of nucleation (W)
R = Freezing front rate (m/s)
R_g = Perfect gas constant (J/(kmol K))
s = Thickness of undercooled zone (m)
T = Temperature (K)
t = Time (s)
T^* = Temperature in supercooled liquid (K)
T° = Homogeneous undercooled temperature (K)
T_f = Freezing front temperature (K)
T_n = Nucleation temperature (°C)
T_s = Sublimation front temperature (K)
X_{ice} = Ice fraction
v = Freezing front velocity (m/s)

Greek letters

ε = Porosity of dried layer
λ = Water molecules mean free path (m)
ρ = Density (kg/m^3)
τ = Tortuosity factor
Ω = Total flow contribution

Subscripts

apparent = Apparent
liquid = Liquid zone
ice = Frozen zone

Literature Cited

1. Kochs M, Korber CH, Heschel I, Nunner B. The influence of the freezing process on vapour transport during sublimation in vacuum-freeze-drying. *Int J Heat Mass Transfer*. 1991;34:2395–2408.
2. Kochs M, Korber CH, Heschel I, Nunner B. The influence of the freezing process on vapour transport during sublimation in vacuum-freeze-drying of macroscopic samples. *Int J Heat Mass Transfer*. 1993;36:1727–1738.
3. Searles JA, Carpenter JF, Randolph TW. The ice nucleation temperature determines the primary drying rate of lyophilization for samples frozen on a temperature-controlled shelf. *J Pharm Sci*. 2001;90:860–871.

4. Searles JA, Carpenter JF, Randolph TW. Annealing to optimize the primary drying rate, reduce freezing-induced drying rate heterogeneity, and determine Tg' in pharmaceutical lyophilization. *J Pharm Sci*. 2001;90:872–887.
5. Nakagawa K, Hottot A, Vessot S, Andrieu J. Influence of controlled nucleation by ultrasounds on ice morphology of frozen formulations for pharmaceutical proteins freeze-drying. *Chem Eng Proc*. 2006;45:783–791.
6. Faydi E, Andrieu J, Laurent P. Experimental study and modelling of the ice crystal morphology of model standard ice cream. Part I: Direct characterization method and experimental data. *J Food Eng*. 2001;48:283–291.
7. Caillet A, Cogne C, Andrieu J, Laurent P, Rivoire A. Characterization of ice cream structure by direct optical microscopy. Influence of freezing parameters. *Food Sci Technol-Leb*. 2003;36:743–749.
8. Hottot A, Vessot S, Andrieu J. A direct characterization method of the ice morphology. Relationship between mean crystals size and primary drying times of freeze-drying processes. *Drying Technol*. 2004;22:2009–2021.
9. Hottot A, Vessot S, Andrieu J. Determination of mass and heat transfer parameters during freeze-drying cycle of pharmaceutical products. *PDA J Pharm Sci Tech*. 2005;59:138–153.
10. Hottot A, Peczalski R, Vessot S, Andrieu J. Freeze-drying of pharmaceutical proteins in vials: Modeling of freezing and sublimation steps. *Drying Technol*. 2006;24:561–570.
11. Qin FJF, Zhao JC, Russel AB, Chen XD, Chen JJ, Robertson L. Simulation and experiment of the unsteady heat transport in the onset time of nucleation and crystallization of ice from the subcooled solution. *Int J Heat Mass Transfer*. 2003;46:3221–3231.
12. Lunardini VJ. *Finite Difference Method for Freezing and Thawing in Heat Transfer in Cold Climates*. Van Nostrand Reinhold Company, 1981.
13. Fenema OR, Powrie WD, Marth EH. *Low-Temperature Preservation of Food and Living Matter*. New York: Marcel Dekker, 1973.
14. Hottot A, Vessot S, Andrieu J. Determination of mass and heat transfer parameters during freeze-drying cycle of pharmaceutical products. *PDA J Pharm Sci Tech*. 2005;59:138–153.
15. Kurz W, Fisher DJ. *Fundamentals of Solidification*, *3rd ed*. Swizerland: Trans Tech Publications, 1992.
16. Bomben JL, King CJ. Heat and mass transport in the freezing of apple tissue. *J Food Technol*. 1982;17:615–632.
17. Reid DS. Cryomicroscope studies of the freezing of model solutions of cryobiological interest. *Cryobiology*. 1984;21:60–67.
18. Woinet B, Andrieu J, Laurent M, Min SG. Experimental and theoretical study of model food freezing. Part II: Characterization and modeling of the ice crystal size. *J Food Eng*. 1998;35:395–407.
19. Pikal MJ, Shah S, Senior D, Lang JE. Physical chemistry of freeze-drying: Measurement of sublimation rates for frozen aqueous solution by a microbalance technique. *J Pharm Sci*. 1983;72:635–650.
20. Simatos D, Blond G, Dauvois P, Sauvageot F. *La Lyophilisation—Principes et Applications*. France: Collection de l'A.N.R.T., 1973.

Manuscript received May 8, 2006, and revision received Jan. 19, 2007.